Positive Low Cloud Feedback Primarily Caused by Increasing Longwave Radiation from the Sea Surface in Two Versions of a Climate Model

Tomoo Ogura[1], Mark J. Webb[2], and Adrian P. Lock[2]

[1]National Institute for Environmental Studies, Tsukuba, Japan.

[2]Met Office Hadley Centre, Exeter, United Kingdom.

Corresponding author: Tomoo Ogura (ogura@nies.go.jp)

Key Points:

- The increase in longwave radiation from the sea surface is a leading order cause of the positive low cloud feedback in a climate model.
- This increase in longwave radiation leads to warming and drying in the boundary layer, which contributes to the decrease in the low cloud.
- This mechanism is not associated with increases in surface evaporation or vertical moisture contrast.

Abstract

Low cloud feedback in global warming projections by climate models is characterized by its positive sign, the mechanism of which is not well understood. Here we propose that the positive sign is primarily caused by the increase in upward longwave radiation from the sea surface. We devise numerical experiments that enable separation of the feedback into components coming from physically distinct causes. Results of these experiments with a climate model indicate that increases in upward longwave radiation from the sea surface cause warming and absolute drying in the boundary layer, leading to the positive low cloud feedback. The absolute drying results from decrease in surface evaporation, and also from decrease in inversion strength which enhances vertical mixing of drier free tropospheric air into the boundary layer. This mechanism is different from previously proposed understanding that positive low cloud feedback is caused by increases in surface evaporation or vertical moisture contrast.

Plain Language Summary

We project future climate change induced by atmospheric greenhouse gas increases by conducting numerical simulations using specialized computer codes, namely Global Climate Models. Results of such simulations are characterized by decreases in low cloud with warming at the Earth's surface, which amplifies the warming by reflecting less sunlight back to space and allowing more sunlight to be absorbed at the surface. This amplifying effect, called 'positive low cloud feedback', is important because the amount of future warming affects our living and safety. However, the mechanism of the low cloud decreases with warming is not well understood. Here we propose that the low cloud decrease is primarily caused by increase in upward longwave radiation from the sea surface. We devise numerical simulations that enable the separation of the low cloud feedback into components coming from physically distinct causes. Results of the simulations indicate that increases in upward longwave radiation from the sea surface cause warming and drying near the Earth's surface, leading to the low cloud decrease. This mechanism is different from previously proposed understanding that the low cloud decrease is due to increases in sea surface evaporation or vertical moisture contrast.

1 Introduction

Low cloud feedback is an important source of uncertainty in the projections of future climate using general circulation models (GCMs). The projections of future climate by multiple GCMs exhibit large inter-model differences, which cause difficulty in evaluating the impact of climate change. The inter-model difference in the projected surface air temperature for a given CO_2 increase is mainly attributable to the inter-model difference in cloud feedback (e.g., Caldwell et al. 2016; Vial et al. 2013; Webb et al. 2013). Specifically, changes in low cloud induced by surface warming make the largest contribution to this uncertainty (e.g., Zelinka et al. 2016, 2020). Understanding the inter-model difference in low cloud feedback is thus imperative, which motivates research on the mechanism of the low cloud feedback simulated by the GCMs.

An interesting feature of the low cloud feedback simulated by the GCMs is that it is positive in most models (Zelinka et al. 2020). The positive sign is associated with decreases in low cloud amount with surface warming, which amplifies the warming by allowing more solar radiation to be absorbed at the surface. However, the magnitude of the low cloud decrease varies widely across models, leading to a large uncertainty in the low cloud feedback. A critical

question here is why low cloud decreases with surface warming, the mechanism of which is not well understood (Boucher et al. 2013; Forster et al. 2021).

Several studies have been conducted to address this issue by attributing simulated changes in low cloud to changes in environmental factors (Qu et al. 2014, 2015; Zhai et al. 2015; Myers and Norris 2016; Brient and Schneider 2016; McCoy et al. 2017; Klein et al. 2017). Qu et al. (2014), among others, developed a heuristic model which interprets the positive low cloud feedback in the subtropical low cloud regions in GCMs. The model indicates that changes in low cloud amount mainly come from two factors: local SST warming and increase in the strength of the inversion capping the atmospheric boundary layer, which is measured by the Estimated Inversion Strength (EIS, Wood and Bretherton 2006). The local SST warming tends to decrease low cloud, while the enhancement of EIS tends to increase the cloud. The net effect is a decrease in low cloud amount because the effect of the SST outweighs that of the EIS in most models.

The mechanism underlying the effect of EIS on low cloud is well understood (Klein and Hartmann 1993; Wood and Bretherton 2006). However, the mechanism of how the local SST warming influences the low cloud is still under debate. The following two mechanisms have been proposed, based on studies using Large Eddy Simulations. First, SST warming leads to an increase in surface latent heat flux, which enhances vertical mixing by turbulence or convection in the lower troposphere. This enhances entrainment of drier air from the free troposphere into the moister boundary layer, desiccating low cloud (Rieck et al. 2012). Second, the increase in latent heat flux from the sea surface induces an increase in water vapor specific humidity in the atmosphere. The magnitude of the increase in humidity is more pronounced in the boundary layer than in free troposphere, increasing the vertical moisture contrast. This increase in moisture contrast enhances the efficiency with which vertical mixing dehydrates the boundary layer, reducing low cloud (Bretherton and Blossey 2014, Sherwood et al. 2014, van der Dussen et al. 2015).

Recently, however, detailed examination of some GCM experiments gave results which are not consistent with the above understanding. For instance, Webb et al. (2018) explored the impact of surface latent heat flux on low cloud amount, forcing the latent heat flux to increase at different rates with SST warming in HadGEM2-A. They found that the magnitude of the low cloud decrease becomes smaller when the latent heat flux is forced to increase at higher rates. Similar results were obtained by Watanabe et al. (2018) using MIROC5. These findings suggest that mechanisms other than the increase in latent heat flux are needed to explain the decrease in low cloud with SST warming in climate models. However, such mechanisms are yet to be identified. Here we propose an alternative mechanism for the low cloud decrease with SST warming based on a new method for decomposing feedbacks in GCM experiments. We argue that the increase in upward longwave radiation from the sea surface is a leading order cause of the low cloud decrease.

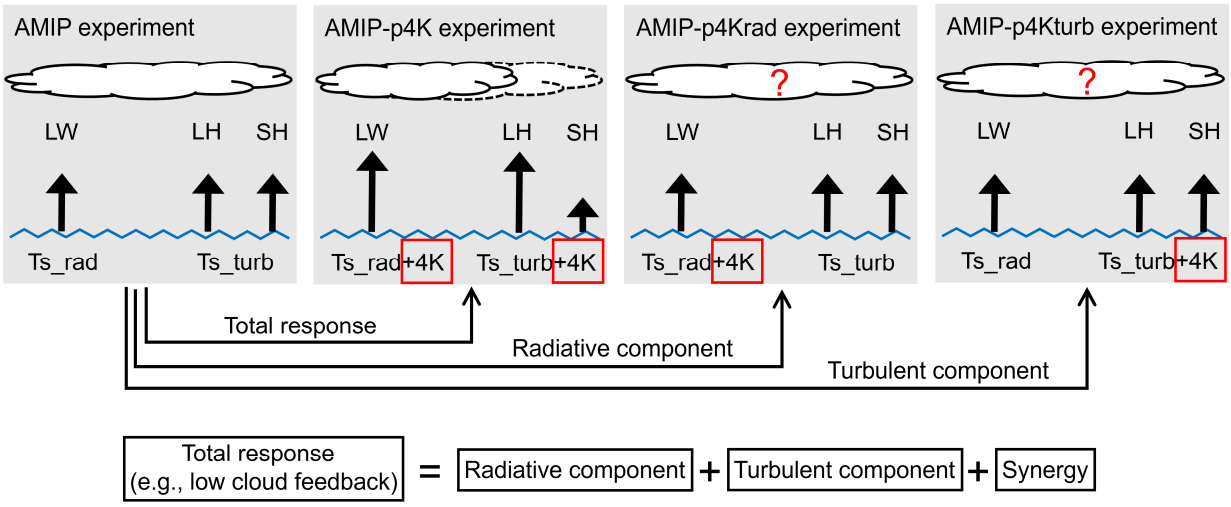

Figure 1. Schematic showing the experimental design. Ts_rad indicates the SST used for calculating LW radiation from the sea surface. Ts_turb is the SST used for calculating turbulent transport from the sea surface, including latent heat (LH) and sensible heat (SH) fluxes.

2 Numerical experiments

The low cloud feedback is investigated using an atmospheric GCM MIROC6 with the spatial resolution of T85 (~1.4˚) with 81 vertical levels (Tatebe et al. 2019). The simulation protocol follows that of the Atmospheric Model Intercomparison Project (AMIP), because the AMIP-type experiments can simulate the low cloud changes that are caused by the SST warming, which are the main focus of this study. They also provide a good approximation to the cloud feedbacks determined from coupled atmosphere-ocean CO_2-forced simulations (Ringer et al. 2014).

In the AMIP-p4K run, the uniform SST warming of 4K compared to the AMIP run modifies the atmosphere via two causal pathways, firstly by increasing the upward longwave radiation from the sea surface, and secondly by changing the turbulent transport at the air-sea interface, such as the latent and sensible heat fluxes (Figure 1). The decrease in low cloud amount, and hence the positive low cloud feedback, is a result of these two causal factors.

We attempt to better understand the roles of the two factors by adding two experiments. In the first experiment, SST is raised by 4K only when calculating the upward longwave radiation from the sea surface using Planck function (AMIP-p4Krad experiment, Figure 1). In the second, SST is raised by 4K only when calculating the turbulent transport at the air-sea interface using bulk aerodynamic formulas (AMIP-p4Kturb experiment). More details of the two experiments are given in the Supporting Information (Text S1). All of the experiments are integrated for 1979-2014 and the output is averaged for 36 years.

The differences of the SST warming experiments compared to the AMIP run are called 'total response (AMIP-p4K minus AMIP)', 'radiative component (AMIP-p4Krad minus AMIP)', and 'turbulent component (AMIP-p4Kturb minus AMIP)', respectively. As the total response, we focus on the low cloud feedback, and write it as a sum of the radiative component, the turbulent component, and a synergy term (Figure 1). Now the low cloud feedback is separated into

components that originate from physically distinct causes, namely, the effect of increasing SST on upwelling surface longwave radiation and its effect on surface turbulent fluxes. The intention here is to see which component makes the low cloud feedback positive. The synergy is a residual term that is evaluated as the difference between the total response and the sum of the radiative and turbulent components. It represents the effect of the radiative and turbulent components working together.

All of the experiments, as outlined above, are repeated using another atmospheric GCM MIROC5 with the spatial resolution of T42 (~2.8˚) with 40 vertical levels (Shiogama et al. 2012; Ogura et al. 2017). In the following, however, we present the output of MIROC6 only, since the results from MIROC5 are similar to those from MIROC6. Results from MIROC5 are shown in the Supporting Information so that readers can confirm robustness of the conclusions (Figures S1-S3).

3 Results

We first present the low cloud feedback simulated by MIROC6 in Figure 2(a). This is evaluated by multiplying changes in the ISCCP low cloud amount by the cloud radiative kernel, which gives the changes in radiation flux at the TOA induced by the low cloud changes (Zelinka et al. 2012; Bodas-Salcedo et al. 2011; Klein and Jakob 1999; Webb et al. 2001). The ISCCP cloud amount with cloud top pressure greater than 680hPa is used for the evaluation. In Figure 2(a), we confirm that the global average low cloud feedback is positive. The positive signal is particularly evident in subtropical marine regions off the western coasts of continents, where low clouds prevail in both observations and model control climates.

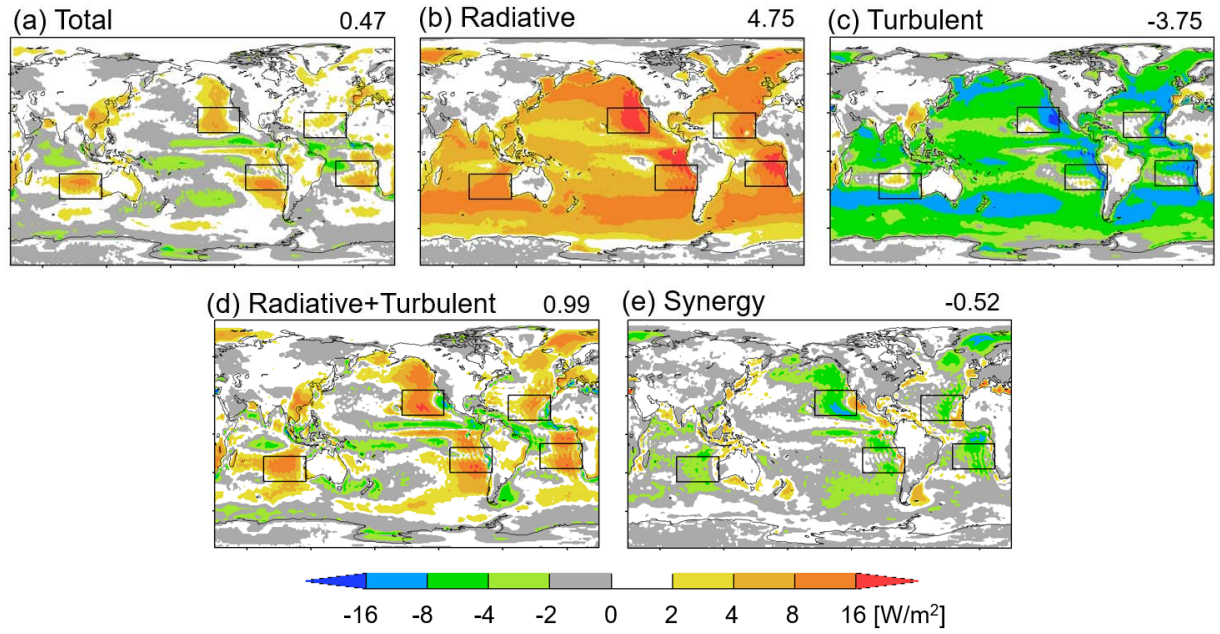

Figure 2. Low cloud feedback induced by 4K increases in SST. (a) Total low cloud feedback, (b) radiative component, (c) turbulent component, (d) sum of the radiative and turbulent components, and (e) synergy. Global averages are indicated at the top right of each panel. The

151 units can be converted to [W/m^2/K] by dividing by the surface warming of 4.54K in the AMIP-
152 p4K run. Black rectangles indicate low cloud regions focused on in Figures 3 and 4.

153

154 The low cloud feedback is separated into the radiative component, turbulent component,
155 and synergy as shown in Figure 2(b,c,e). The radiative component is characterized with positive
156 contributions over the oceans, while the turbulent component is dominated by negative
157 contributions (Figure 2b,c). If we add the two components together, as shown in Figure 2(d), the
158 result captures the geographical pattern (especially the sign) of the total low cloud feedback in
159 Figure 2(a). The pattern correlation between Figures 2(a) and 2(d) is 0.81. Therefore, the low
160 cloud feedback can be approximated as a sum of the radiative and turbulent components,
161 although the synergy effect is not negligible as shown in Figure 2(e).

162 Focusing on the sum of the radiative and the turbulent components in Figure 2(d), we
163 find that the low cloud feedback becomes positive where the radiative component outweighs the
164 turbulent component. Without the radiative component, the low cloud feedback would have been
165 negative overall (Figure 2c). This means that the low cloud feedback becomes positive because
166 of the radiative component. In other words, the positive sign of the feedback is mainly attributed
167 to the increase in upward longwave radiation from the sea surface.

168 How does the longwave radiation cause the positive low cloud feedback? The mechanism
169 is further examined, focusing on area averages over the five oceanic regions indicated by the
170 black rectangles in Figure 2. These regions are chosen because the positive low cloud feedback
171 stands out here in MIROC6 (Figure 2a), and also because they match the low cloud regions
172 based on observations (Qu et al. 2014). Here, vertical profiles of cloud-related variables are
173 examined in Figure 3. We focus on the cloud amount below the 680hPa level because this is
174 where the low cloud feedback originates (Figure 3a,e). Note also that the low cloud feedback is
175 strongly correlated with the cloud amount, but less well with the cloud optical thickness or cloud
176 top pressure (Figure S4).

177 The total response of the cloud amount below the 680hPa level (Figure 3e, black) shows
178 a characteristic dipole pattern, in which a cloud decrease above (σ-p level$\approx$0.85) is moderated
179 by a cloud increase below (σ-p level$\gtrsim$0.9). The dipole pattern reflects shallowing of the
180 boundary layer cloud at σ-p level$\approx$0.9 (Figure 3a). As a comparison, we also plot the radiative
181 and turbulent components in Figure 3e (red and blue). Clearly, the turbulent component (blue)
182 fails to reproduce the total response (black) at the σ-p level$\gtrsim$0.9, namely, the blue curve
183 exceeds the black one. This explains how the turbulent component shows increase in low cloud,
184 leading to the negative feedback. In contrast, the radiative component (red) shows a decrease in
185 low cloud at σ-p level$\approx$0.9, which opposes the cloud increase in the turbulent component (blue).
186 When added together, the radiative and turbulent components (green) roughly reproduce the
187 dipole pattern in the total response (black), although the positive and negative maxima are
188 exaggerated. Hence, the low cloud decrease in the radiative component (red) is the key to
189 understanding the low cloud decrease in the total response (black).

190 The low cloud decrease in the radiative component (Figure 3e, red) is consistent with a
191 decrease in relative humidity (Figure 3f, red), which comes from both a warming and a decrease
192 in specific humidity (Figure 3gh, red). This can be confirmed by looking at the geographical

distribution (Figure S5). The warming is caused by the increase in upward longwave radiation from the sea surface, which is absorbed by the atmosphere (Figure 3i). The decrease in specific humidity can be explained by two mechanisms. Firstly, the magnitude of the warming is larger in the boundary layer compared to the free troposphere, having a bottom-heavy vertical profile (Figure 3h, red). This decreases the strength of the inversion capping the boundary layer. As a result, vertical mixing across the inversion increases, making the boundary layer less humid (Klein and Hartmann 1993). Secondly, the longwave-induced warming of the atmosphere increases the static stability at the air-sea interface. Note that the SST is kept the same as the AMIP experiment except for calculating the upward longwave radiation. The increase in the static stability suppresses the turbulent transport of water vapor from the sea surface (Text S2, Figure S9).

The warming and the absolute drying in the boundary layer, as described above, leads to the low cloud decrease in the radiative component. The mechanism may be summarized as "Cloud Reduction due to Increased Surface Temperature Longwave Emission (CRISTLE)". In addition, the decrease in the low cloud initiates a process that reduces the low cloud further. Namely, the decrease in the low cloud causes weakening of the radiative cooling of the boundary layer (Figure S8d,f, black). This contributes to warming and a decrease in relative humidity, thereby reducing the low cloud further (Figure S7e, green, Brient and Bony 2012). We note that the low cloud decrease in the radiative component is not associated with an increase in specific humidity or surface evaporation (Figures 3g, S9a). We also considered a number of other possible explanations for the low cloud reductions in the radiative component (Table S1).

In the turbulent component, by contrast, the low cloud changes are associated with the increase in specific humidity and surface evaporation. We attribute the low cloud increases in the turbulent component to multiple processes that compete with each other, as in Vial et al. (2016). For instance, the magnitude of the increase in specific humidity is larger at lower altitudes, which enhances the moisture contrast between the free troposphere and the boundary layer (Figure 3g, blue). As a result, the upward moisture flux by shallow convection increases, which tends to decrease the low cloud (Figures S6c,f, red, Zhang et al. 2013). In contrast, we also note that the vertical temperature profile stabilizes with warming, which increases strength of the inversion capping the boundary layer (Figure 3h, blue). As a result, vertical mixing across the inversion reduces, which tends to keep the boundary layer more humid and increase the low cloud (Miller 1997). Understanding the roles of different processes within the turbulent component will be a subject of future studies. More details of the competing processes are given in Table S1.

The results obtained so far illustrate how the low cloud feedback originates from the sea surface warming. The processes involved in the feedback are classified into the radiative and the turbulent components. The two components are dissimilar to each other, with the former decreasing the ISCCP low cloud amount (LCA), while the latter increases it. However, the two components are both related to changes in the EIS, as follows. In the radiative component, the LCA decreases as the EIS decreases (Figure 3e,h, red). In the turbulent component, the LCA increases as the EIS increases (Figure 3e,h, blue). In the synergy component, also, the LCA increases as the EIS increases (not shown). The relationship between the LCA and the EIS is qualitatively consistent with observation (Wood and Bretherton 2006; Klein and Hartmann 1993).

If we add the three components together, however, the relation between the LCA and the EIS changes compared to that above. Namely, the LCA decreases as the EIS increases (Figure

3e,h, black), which may appear counter-intuitive. Why does the relation between the LCA and the EIS break down when the components are added together? This issue is examined in Figure 4(a).

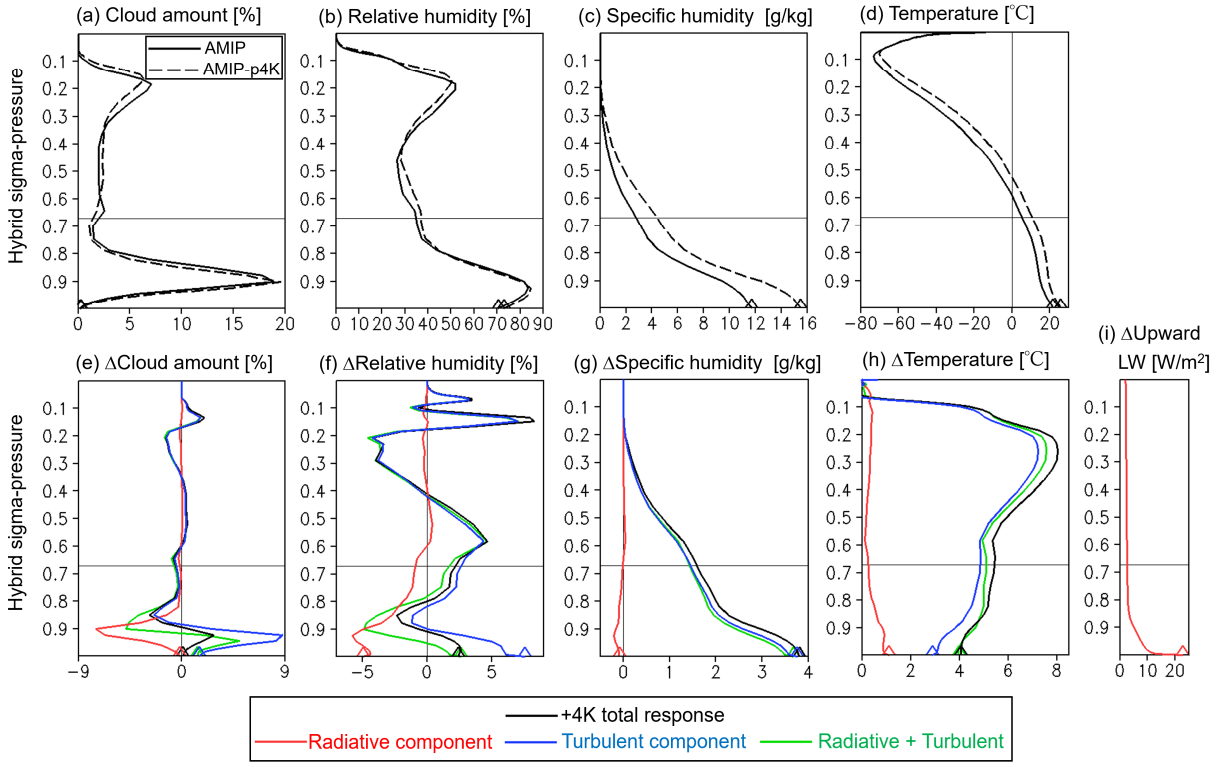

Figure 3. Vertical profiles of cloud-related variables averaged over the low cloud regions indicated by the black rectangles in Figure 2. (a)(b)(c)(d) for AMIP and AMIP-p4K experiments, and (e)(f)(g)(h)(i) for changes due to +4K SST warming. The vertical coordinate is hybrid σ-p on model level. Horizontal lines at the σ-p level of 0.67 mark the boundary between low-top clouds and middle-top clouds at 680hPa. Diamonds indicate values at the lowest level. The changes in upward longwave, (i), are evaluated assuming that the atmosphere remains fixed at the AMIP condition.

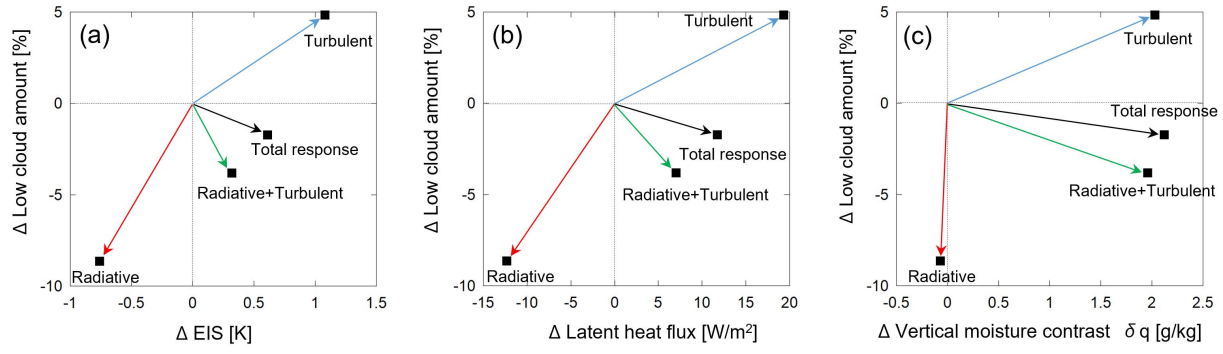

Figure 4 Relationships between changes in low cloud amount and changes in (a) EIS, (b) latent heat flux, and (c) vertical moisture contrast δq. The δq is defined as the specific humidity q at 1000hPa minus q at 700 hPa. The delta, Δ, denotes changes induced by the SST warming of 4K. The data are averages over the low cloud regions indicated by the black rectangles in Figure 2.

In figure 4(a), the changes induced by the SST warming of 4K are represented by 2-D vectors on the ΔEIS-ΔLCA plane. The radiative component is shown in red, with the coordinate values of $(\Delta EIS_{rad}, \Delta LCA_{rad})$, while the turbulent component is shown by blue, with the coordinate values of $(\Delta EIS_{turb}, \Delta LCA_{turb})$. The two vectors appear in the 3rd and the 1st quadrants, indicating that the LCA decreases (increases) as the EIS decreases (increases). Adding the two components together, we obtain the sum shown by green, with the coordinate values of $(\Delta EIS_{turb} + \Delta EIS_{rad}, \Delta LCA_{turb} + \Delta LCA_{rad})$. Now the vector appears in the 4th quadrant, indicating that the LCA decreases as the EIS increases, which captures the sign of the total response shown in black.

Focusing on the sum of the two components, we find that the LCA decreases as the EIS increases under the following conditions:

$$\Delta EIS_{turb} + \Delta EIS_{rad} > 0 \, , and \; \Delta LCA_{turb} + \Delta LCA_{rad} < 0 \qquad (1).$$

Namely, the change in the EIS is dominated by the turbulent component, while the change in the LCA is dominated by the radiative component. In other words, the total response to the SST warming includes two counter-acting components, and which component dominates depends on the variable we look at. This explains how the relation between the LCA and the EIS changes when adding the radiative and turbulent components together.

We also note that rate of change in the LCA with respect to the EIS is different between the radiative and turbulent components, as follows:

$$\Delta LCA_{rad}/\Delta EIS_{rad} > \Delta LCA_{turb}/\Delta EIS_{turb} \qquad (2).$$

The conditions (1) can be met only under the condition (2). The condition (2) indicates that LCA is less sensitive to EIS in the turbulent component than in the radiative component. This may be because, in the turbulent component, the EIS increase is accompanied by an increase in vertical moisture contrast, δq (Figure 3gh, blue). The change in the EIS tends to increase the LCA, while the change in the δq tends to decrease it, making the LCA less sensitive to the EIS (Kawai et al. 2017).

Similar arguments hold, even if we replace the EIS with the surface latent heat flux or the vertical moisture contrast, δq (Figure 4b,c). Namely, in the total response shown in black, the LCA decrease is accompanied by an increase in latent heat flux or δq. This can be explained by the fact that the LCA decrease is dominated by the radiative component while the increase in latent heat flux or δq is driven by the turbulent component.

4 Conclusions

In order to understand the reason for the positive sign of the low cloud feedback simulated by GCMs, we devise numerical experiments which enable separation of the feedback into a component driven by upward surface longwave radiation and another driven by surface turbulent fluxes. The numerical experiments are conducted using MIROC5 and MIROC6. The results indicate that the positive sign of the low cloud feedback is mainly attributed to the increase in longwave radiation from the sea surface, which leads to a warming and a drying in the boundary layer, as well as a decrease in the low cloud amount (LCA). The mechanism involved is summarized as "Cloud Reduction due to Increased Surface Temperature Longwave Emission (CRISTLE)". It is not associated with increases in surface latent heat flux or vertical moisture contrast. The decomposition of the feedback also helps to explain how the LCA decrease is accompanied by increases in the EIS, the latent heat flux, and the vertical moisture contrast.

In addition, the obtained results indicate that changes in the turbulent fluxes tend to increase the LCA, thereby making the feedback more negative in MIROC5 and MIROC6. The results are consistent with the idea that changes in the turbulent fluxes are an important factor that controls the low cloud feedback. The cloud feedback is affected by changes in the turbulent fluxes in remote regions as well as the changes below the low clouds. Indeed, the changes in the turbulent fluxes and the upward surface longwave radiation are both needed to explain the geographical pattern of the low cloud feedback.

Whether other GCMs or Large Eddy Simulations support the present findings will be an interesting topic for future studies. Currently, output from CMIP6 experiments is analyzed to see if the mechanism proposed in this study can explain the sub-tropical low cloud feedbacks in multi-GCMs. In addition, the experiments proposed in this study are being conducted with Large Eddy Simulations under the CGILS protocol (Blossey et al. 2016). The results will be presented in subsequent papers.

Acknowledgments

This study was funded by the Integrated Research Program for Advancing Climate Models (Grant Number JPMXD0717935457) and the Program for the Advanced Studies of Climate Change Projection (Grant Number JPMXD0722680395) from the Ministry of Education, Culture, Sports, Science and Technology, Japan. Mark Webb was funded by the UK BEIS/Defra Met Office Hadley Centre Climate Programme (GA01101). Simulations were performed with the NIES supercomputer system and the Earth Simulator at JAMSTEC. We thank Mark D. Zelinka for providing cloud radiative kernel, and Tokuta Yokohata and Koji Ogochi for implementing COSP in MIROC5. Figures in this paper were plotted using Grid Analysis and Display System (GrADS). Data used in this study are archived at https://doi.org/10.5281/zenodo.4153249.

References

Blossey, P. N., C. S. Bretherton, A. Cheng, S. Endo, T. Heus, A. P. Lock, and J. J. van der Dussen (2016), CGILS Phase 2 LES intercomparison of response of subtropical marine low

cloud regimes to CO_2 quadrupling and a CMIP3 composite forcing change, *J. Adv. Model. Earth Syst.*, 08, doi:10.1002/2016MS000765.

Boucher, O., D. Randall, P. Artaxo, C. Bretherton, G. Feingold, P. Forster, V. -M. Kerminen, Y. Kondo, H. Liao, U. Lohmann, P. Rasch, S. K. Satheesh, S. Sherwood, B. Stevens, and X. Y. Zhang (2013), Clouds and Aerosols. In:*Climate Change 2013:The Physical Science Basis. Contribution of Working Group 1 to the Fifth Assessment Report of the Intergovernmental Panel on Climate Change* [Stocker, T. F., D. Qin, G. -K. Plattner, M. Tignor, S. K. Allen, J. Boschung, A. Nauels, Y. Xia, V. Bex, and P. M. Midgley (eds.)]. Cambridge University Press, Cambridge, United Kingdom and New York, NY, USA.

Bodas-Salcedo, A., M. J. Webb, S. Bony, H. Chepfer, J. -L. Dufresne, S. A. Klein, Y. Zhang, R. Marchand, J. M. Haynes, R. Pincus, and V. O. John (2011), COSP Satellite simulation software for model assessment, *Bull. Amer. Meteor. Soc.*, 92, 1023–1043, doi:10.1175/2011BAMS2856.1.

Bretherton, C. S. and P. N. Blossey (2014), Low cloud reduction in a greenhouse-warmed climate: Results from Lagrangian LES of a subtropical marine cloudiness transition, *J. Adv. Model. Earth Syst*., 6, doi:10.1002/2013MS000250.

Brient, F. and S. Bony (2012), How may low-cloud radiative properties simulated in the current climate influence low-cloud feedbacks under global warming? *Geophys. Res. Lett.*, 39, L20807, doi:10.1029/2012GL053265.

Brient, F. and T. Schneider (2016), Constraints on climate sensitivity from space-based measurements of low-cloud reflection, *J. Clim.*, 29, 5821–5835, doi:10.1175/JCLI-D-15-0897.1.

Caldwell, P. M., M. D. Zelinka, K. E. Taylor and K. Marvel (2016), Quantifying the sources of intermodal spread in equilibrium climate sensitivity, *J. Clim.*, 29, 513–524, doi:10.1175/JCLI-D-15-0352.1.

Forster, P., T. Storelvmo, K. Armour, W. Collins, J.-L. Dufresne, D. Frame, D. J. Lunt, T. Mauritsen, M. D. Palmer, M. Watanabe, M. Wild, and H. Zhang (2021), The Earth's Energy Budget, Climate Feedbacks, and Climate Sensitivity. In *Climate Change 2021: The Physical Science Basis. Contribution of Working Group 1 to the Sixth Assessment Report of the Intergovernmental Panel on Climate Change* [Masson-Delmotte, V., P. Zhai, A. Pirani, S. L.

Connors, C. Péan, S. Berger, N. Caud, Y. Chen, L. Goldfarb, M. I. Gomis, M. Huang, K. Leitzell,

E. Lonnoy, J. B. R. Matthews, T. K. Maycock, T. Waterfield, O. Yelekçi, R. Yu, and B. Zhou (eds.)]. Cambridge University Press, Cambridge, United Kingdom and New York, NY, USA, pp.923-1054, doi:10.1017/9781009157896.009.

Kawai, H., T. Koshiro, and M. J. Webb (2017), Interpretation of factors controlling low cloud cover and low cloud feedback using a unified predictive index, *J. Clim.*, 30, 9119-9131, doi:10.1175/JCLI-D-16-0825.1.

Klein, S. A., and D. L. Hartmann (1993), The seasonal cycle of low stratiform clouds, *J. Clim.*, 6, 1587–1606.

Klein, S. A., and C. Jakob (1999), Validation and sensitivities of frontal clouds simulated by the ECMWF model, *Mon. Wea. Rev.*, 127, 2514–2531.

Klein, S. A., A. Hall, J. R. Norris, and R. Pincus (2017), Low-cloud feedbacks from cloud-controlling factors: a review, *Surv. Geophys.*, 38, 1307–1329, doi:10.1007/s10712-017-9433-3.

McCoy, D. T., R. Eastman, D. L. Hartmann, and R. Wood (2017), The change in low cloud cover in a warmed climate inferred from AIRS, MODIS, and ERA-Interim, *J. Clim.*, 30, 3609-3620, doi:10.1175/JCLI-D-15-0734.1.

Miller, R. L. (1997), Tropical thermostats and low cloud cover, *J. Clim.,* 10, 409-440.

Myers, T. A., and J. R. Norris (2016), Reducing the uncertainty in subtropical cloud feedback, *Geophys. Res. Lett.*, 43, doi:10.1002/2015GL067416.

Narenpitak, P., and C. S. Bretherton (2019), Understanding negative subtropical shallow cumulus cloud feedbacks in a near-global aquaplanet model using limited area cloud-resolving simulations, *J. Adv. Model. Earth Syst.,* 11, 1600-1626, doi:10.1029/2018MS001572.

Ogura, T., H. Shiogama, M. Watanabe, M. Yoshimori, T. Yokohata, J. D. Annan, J. C. Hargreaves, N. Ushigami, K. Hirota, Y. Someya, Y. Kamae, H. Tatebe, and M. Kimoto (2017), Effectiveness and limitations of parameter tuning in reducing biases of top-of-atmosphere radiation and clouds in MIROC version 5, *Geosci. Model Dev.*, 10, 4647-4664, doi:10.5194/gmd-10-4647-2017.

Qu, X., A. Hall, S. A. Klein, and P. M. Caldwell (2014), On the spread of changes in marine low cloud cover in climate model simulations of the 21st century, *Clim. Dyn.*, 42, 2603–2626, doi:10.1007/s00382-013-1945-z.

Qu, X., A. Hall, S. A. Klein, and A. M. DeAngelis (2015), Positive tropical marine low-cloud cover feedback inferred from cloud-controlling factors, *Geophys. Res. Lett.*, 42, 7767–7775, doi:10.1002/2015GL065627.

Rieck, M., L. Nuijens, and B. Stevens (2012), Marine boundary layer cloud feedbacks in a constant relative humidity atmosphere, *J. Atmos. Sci.*, 69, 2538–2550, doi:10.1175/JAS-D-11-0203.1.

Ringer, M. A., T. Andrews, and M. J. Webb (2014), Global-mean radiative feedbacks and forcing in atmosphere-only and coupled atmosphere-ocean climate change experiments, *Geophys. Res. Lett.,* 41, doi:10.1002/2014GL060347.

Sherwood, S. C., S. Bony, and J. -L. Dufresne (2014), Spread in model climate sensitivity traced to atmospheric convective mixing, *Nature*, 505, 37–42, doi:10.1038/nature12829.

Shiogama, H., M. Watanabe, M. Yoshimori, T. Yokohata, T. Ogura, J. D. Annan, J. C. Hargreaves, M. Abe, Y. Kamae, R. O'ishi, R. Nobui, S. Emori, T. Nozawa, A. Abe-Ouchi, and M. Kimoto (2012), Perturbed physics ensemble using the MIROC5 coupled atmosphere-ocean GCM without flux corrections: experimental design and results -parametric uncertainty of climate sensitivity, *Clim. Dyn.*, 39, 3041–3056, doi:10.1007/s00382-012-1441-x.

Tatebe, H., T. Ogura, T. Nitta, Y. Komuro, K. Ogochi, T. Takemura, K. Sudo, M. Sekiguchi, M. Abe, F. Saito, M. Chikira, S. Watanabe, M. Mori, N. Hirota, Y. Kawatani, T. Mochizuki, K. Yoshimura, K. Takata, R. O'ishi, D. Yamazaki, T. Suzuki, M. Kurogi, T. Kataoka, M. Watanabe, and M. Kimoto (2019), Description and basic evaluation of simulated mean state, internal variability, and climate sensitivity in MIROC6, *Geosci. Model Dev.*, 12, 2727–2765, doi:10.5194/gmd-12-2727-2019.

van der Dussen, J. J., S. R. de Roode, S. Dal Gesso, and A. P. Siebesma (2015), An LES model study of the influence of the free tropospheric thermodynamic conditions on the stratocumulus

response to a climate perturbation, *J. Adv. Model. Earth Syst.*, 7, 670–691, doi:10.1002/2014MS000380.

Vial, J., J. -L. Dufresne, and S. Bony (2013), On the interpretation of inter-model spread in CMIP5 climate sensitivity estimates, *Clim. Dyn.*, 41, 3339–3362, doi:10.1007/s00382-013-1725-9.

Vial, J., S. Bony, J.-L. Dufresne, and R. Roehrig (2016), Coupling between lower-tropospheric convective mixing and low-level clouds: Physical mechanisms and dependence on convection scheme, *J. Adv. Model. Earth Syst.*, 8, 1892-1911, doi:10.1002/2016MS000740.

Watanabe, M., T. Suzuki, R. O'ishi, Y. Komuro, S. Watanabe, S. Emori, T. Takemura, M. Chikira, T. Ogura, M. Sekiguchi, K. Takata, D. Yamazaki, T. Yokohata, T. Nozawa, H. Hasumi, H. Tatebe, and M. Kimoto (2010), Improved climate simulation by MIROC5: mean states, variability, and climate sensitivity, *J. Clim.*, 23, 6312–6335, doi:10.1175/2010JCLI3679.1.

Watanabe, M., Y. Kamae, H. Shiogama, A. M. DeAngelis, and K. Suzuki (2018), Low clouds link equilibrium climate sensitivity to hydrological sensitivity, *Nat. Clim. Change*, 8, 901–906, doi:10.1038/s41558-018-0272-0.

Webb, M. J., C. Senior, S. Bony, and J. -J. Morcrette (2001), Combining ERBE and ISCCP data to assess clouds in the Hadley Centre, ECMWF, and LMD atmospheric climate models, *Clim. Dyn.*, 17, 905–922.

Webb, M. J., F. Hugo Lambert, and J. M. Gregory (2013), Origins of differences in climate sensitivity, forcing and feedback in climate models, *Clim. Dyn.*, 40, 677–707, doi:10.1007/s00382-012-1336-x.

Webb, M. J., A. P. Lock, and F. Hugo Lambert (2018), Interactions between hydrological sensitivity, radiative cooling, stability, and low-level cloud amount feedback, *J. Clim.*, 31, 1833–1850, doi:10.1175/JCLI-D-16-0895.1.

Wood, R., and C. S. Bretherton (2006), On the relationship between stratiform low cloud cover and lower-tropospheric stability, *J. Clim.*, 19, 6425–6432, doi:10.1175/JCLI3988.1.

Wyant, M. C., C. S. Bretherton, and P. N. Blossey (2009), Subtropical low cloud response to a warmer climate in a superparameterized climate model. Part 1: Regime sorting and physical mechanisms, *J. Adv. Model. Earth Syst.,* 1, 7, doi:10.3894/JAMES.2009.1.7.

Zhai, C., J. H. Jiang, and H. Su (2015), Long-term cloud change imprinted in seasonal cloud variation: More evidence of high climate sensitivity, *Geophys. Res. Lett.*, 42, 8729-8737, doi:10.1002/2015GL065911.

Zhang, M., C. S. Bretherton, P. N. Blossey, P. H. Austin, J. T. Bacmeister, S. Bony, F. Brient, S. K. Cheedela, A. Cheng, A. D. Del Genio, S. R. De Roode, S. Endo, C. N. Franklin, J.-C. Golaz, C. Hannay, T. Heus, F. A. Isotta, J.-L. Dufresne, I.-S. Kang, H. Kawai, M. Köehler, V. E. Larson, Y. Liu, A. P. Lock, U. Lohmann, M. F. Khairoutdinov, A. M. Molod, R. A. J. Neggers, P. Rasch, I. Sandu, R. Senkbeil, A. P. Siebesma, C. Siegenthaler-Le Drian, B. Stevens, M. J. Suarez, K.-M. Xu, K. von Salzen, M. J. Webb, A. Wolf, and M. Zhao (2013), CGILS: Results from the first phase of an international project to understand the physical mechanisms of low cloud feedbacks in single column models, *J. Adv. Model. Earth Syst.*, 5, 1-17, doi:10.1002/2013MS000246.

Zelinka, M. D., S. A. Klein, and D. L. Hartmann (2012), Computing and partitioning cloud feedbacks using cloud property histograms. Part I:cloud radiative kernels, *J. Clim.*, 25, 3715-3735, doi:10.1175/JCLI-D-11-00248.1.

Zelinka, M. D., C. Zhou, and S. A. Klein (2016), Insights from a refined decomposition of cloud feedbacks, *Geophys. Res. Lett.*, 43, doi:10.1002/2016GL069917.

Zelinka, M. D., T. A. Myers, D. T. McCoy, S. Po-Chedley, P. M. Caldwell, P. Ceppi, S. A. Klein, and K. E. Taylor (2020), Causes of higher climate sensitivity in CMIP6 models. *Geophys. Res. Lett.*, 47, e2019GL085782. doi:10.1029/2019GL085782.

Figure 1.

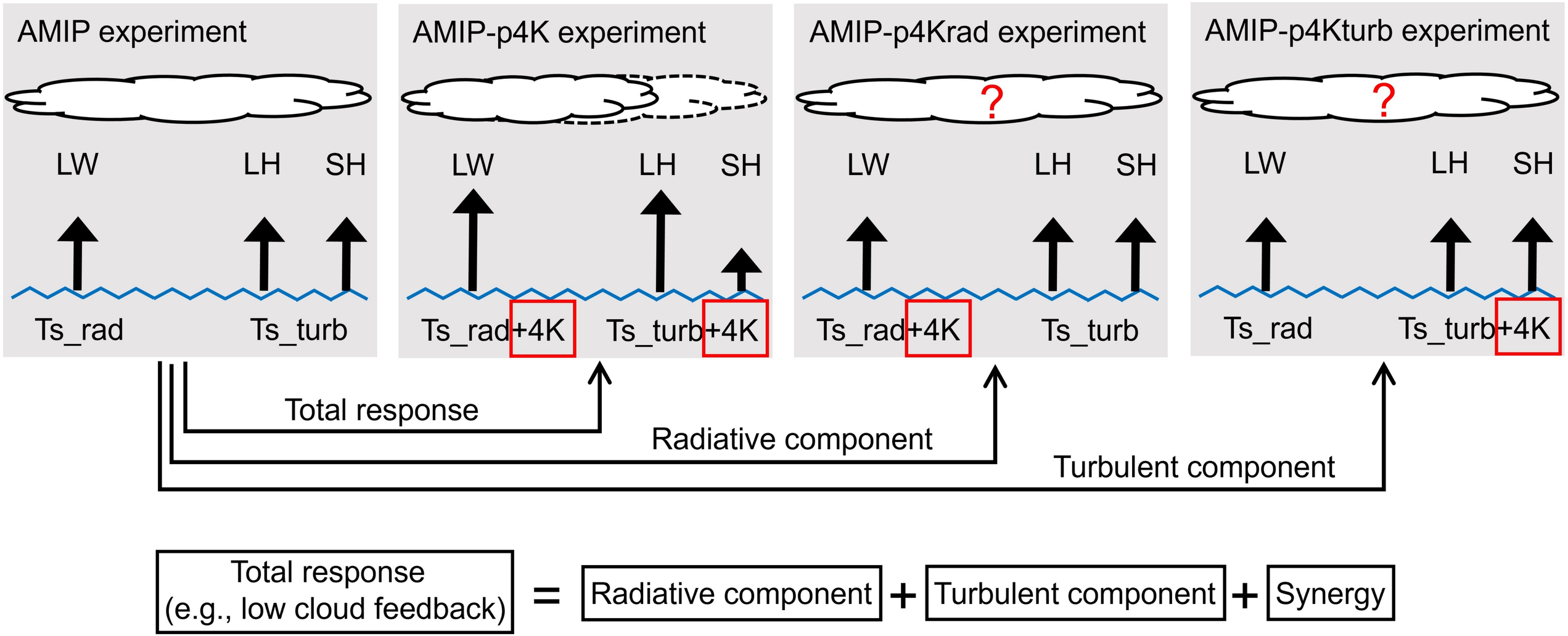
AMIP experiment
LW
LH
SH
Ts_rad
Ts_turb
AMIP-p4K experiment
LW
LH
SH
Ts_rad+4K
Ts_turb+4K
AMIP-p4Krad experiment
?
LW
LH
SH
Ts_rad+4K
Ts_turb
AMIP-p4Kturb experiment
?
LW
LH
SH
Ts_rad
Ts_turb+4K
Total response
Radiative component
Turbulent component
Total response
(e.g., low cloud feedback)
=
Radiative component
+
Turbulent component
+
Synergy

Figure 2.

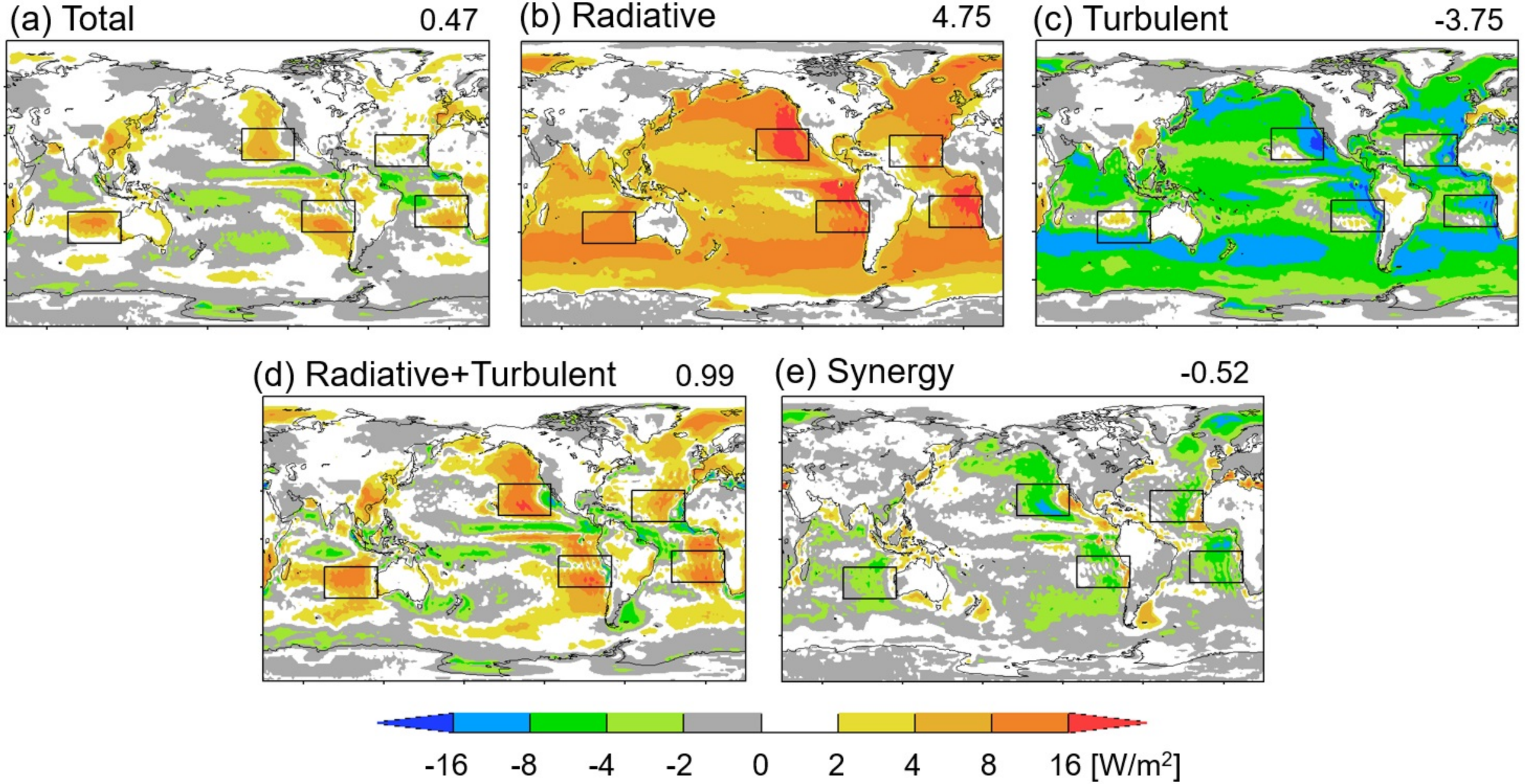
(a) Total
0.47
(b) Radiative
4.75
(c) Turbulent
-3.75
(d) Radiative+Turbulent
0.99
(e) Synergy
-0.52
-16
-8
-4
-2
0
2
4
8
16 [W/m2]

Figure 3.

(a) Cloud amount [%]

(b) Relative humidity [%]

(c) Specific humidity [g/kg]

(d) Temperature [℃]

Hybrid sigma-pressure

AMIP

AMIP-p4K

(e) ΔCloud amount [%]

(f) ΔRelative humidity [%]

(g) ΔSpecific humidity [g/kg]

(h) ΔTemperature [℃]

(i) ΔUpward LW [W/m²]

+4K total response

Radiative component

Turbulent component

Radiative + Turbulent

Figure 4.

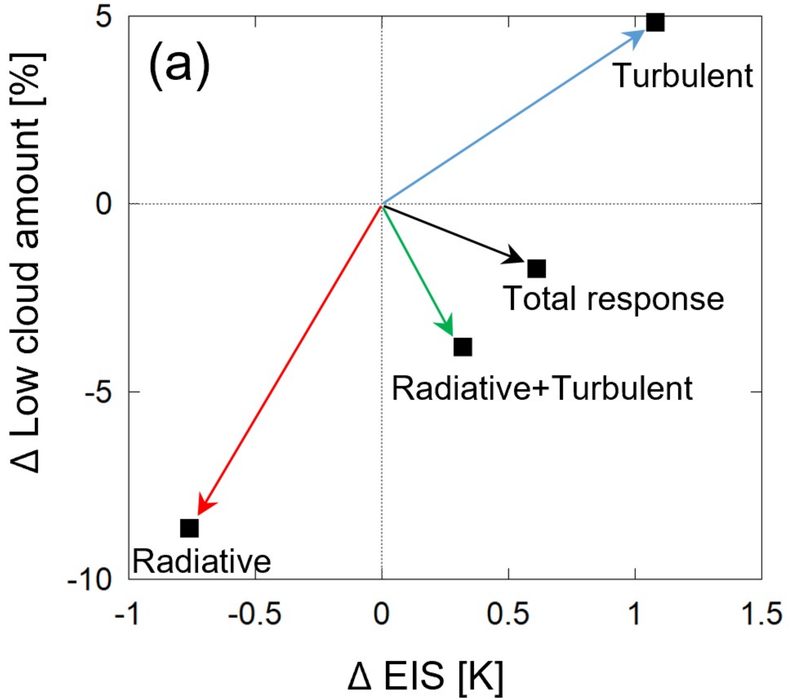
(a)
Turbulent
Total response
Radiative+Turbulent
Radiative
Δ Low cloud amount [%]
Δ EIS [K]
5
0
-5
-10
-1
-0.5
0
0.5
1
1.5

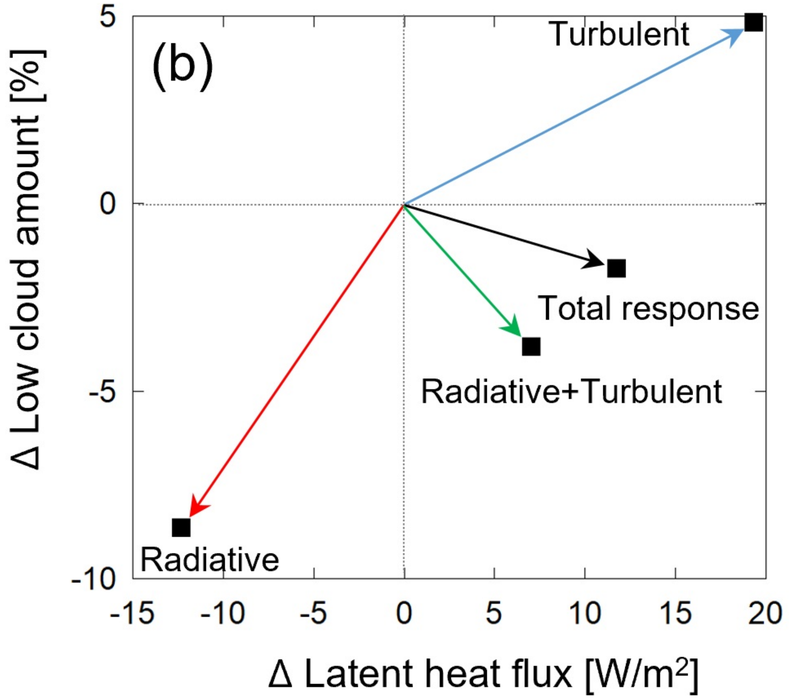
(b)
Turbulent
Total response
Radiative+Turbulent
Radiative
Δ Low cloud amount [%]
Δ Latent heat flux [W/m²]
5
0
-5
-10
-15
-10
-5
0
5
10
15
20

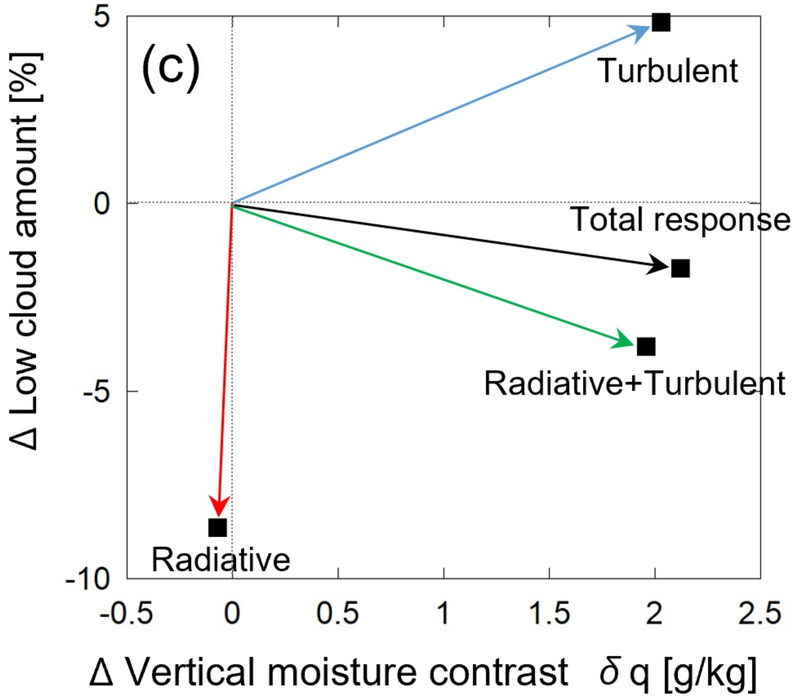
(c)
Turbulent
Total response
Radiative+Turbulent
Radiative
Δ Low cloud amount [%]
Δ Vertical moisture contrast δ q [g/kg]
5
0
-5
-10
-0.5
0
0.5
1
1.5
2
2.5